Research Article | Vol. 30, No. 25 / 5 Dec 2022 / Optics Express 45340
Optics EXPRESS

Optical bistability in PECVD silicon-rich nitride

ALEX FRIEDMAN,* DMITRII BELOGOLOVSKII, ANDREW GRIECO, AND YESHAIAHU FAINMAN

Department of Electrical & Computer Engineering, University of California, San Diego, 9500 Gilman Drive, La Jolla, California 92093, USA
amfriedm@eng.ucsd.edu

Abstract: We present a study of optical bi-stability in a 3.02 refractive index at 1550nm plasma enhanced chemical vapor deposition (PECVD) silicon-rich nitride (SRN) film, as it pertains to bi-stable switching, memory applications, and thermal sensing applications. In this work we utilize an SRN ring resonator device, which we first characterize at low-power and then compare thermo-optic coefficients, $(2.12 \pm 0.125) \times 10^{-4}$/°C, obtained from thermal-heating induced resonance shifts to optically induced resonance shifts as well as estimated propagation loss and absorption. We then measure the time response of this nonlinearity demonstrating the relaxation time to be 18.7 us, indicating the mechanism to be thermal in nature. Finally, we demonstrate bi-stable optical switching.

1. Introduction

Research towards optical logic components is an ongoing area of interest and optically bi-stable devices have been of keen interest in such research as they can provide a fundamental building block for optical logic gates [1–3]. In the past, optical bistability has been shown in silicon devices [4–9]; however, silicon nitride has become an attractive candidate for nonlinear optical processes due to its low-loss nature, low two-photon absorption, and as has more recently been shown, the capability to exhibit an enhanced third order nonlinear susceptibility. Existing work in literature exploring optical bistability in silicon nitride ring resonator devices has primarily focused on stoichiometric to low refractive index silicon nitride [10], both exploring the possibility of a Kerr based ultra-fast optically bistable ring resonator for use as a memory element [11] as well as in a variety of other novel applications such as for a photonic thermometer where thermo-optic bistability is exploited for temperature sensing [12]. In past work by the author's [13], as well as others in the literature [14–18], we have shown how by controlling the conditions during deposition, high silicon content silicon-rich nitride films can be deposited by PECVD and shown that these films exhibit enhanced second and third order nonlinear susceptibilities, thermo-optic coefficient, and refractive index while maintaining many of the benefits of silicon nitride films. Such films have been used in a variety of manners in literature such as for optical parametric amplifiers [19], for soliton-effect optical pulse compression [20], as well as pushes towards the fabrication of even higher composition films such as low temperature plasma-deposited dichlorosilane-based ultra-silicon-rich nitride films [21]. A useful overview of the various forms of silicon-rich nitride as a highly nonlinear CMOS platform can be found in [17].

In this manuscript we demonstrate and characterize thermo-optic bistability in a PECVD SRN with a refractive index of 3.02 at 1500nm for use as an optically bi-stable element. We compare optically induced resonance shifts to thermal heating induced shifts, as well as characterize its time response. Specifically, we determine the thermo-optic coefficient of our PECVD SRN film to be (2.12 ± 0.125)x10^{-4}/°C by examining the optically induced resonance shift. We experimentally demonstrate bi-stable optical switching and measure the time response of the device showing the relaxation time to be approximately 18.7us. Finally, we make an argument for high refractive index PECVD SRN for use as optically bistable material in computing and

#473928 https://doi.org/10.1364/OE.473928
Journal © 2022 Received 24 Aug 2022; revised 19 Oct 2022; accepted 19 Oct 2022; published 30 Nov 2022

Optics EXPRESS

sensing applications such as thermal sensing. Utilizing high refractive index PECVD SRN films for a variety of applications provides significant benefits over traditional utilization of low index or stoichometric nitride films [12] due to the much larger thermo-optic coefficient and higher confinement waveguide while maintaining a low loss guiding layer and negligible TPA [22].

2. Design and fabrication

In this manuscript we characterize the thermo-optic properties of high refractive index PECVD SRN, demonstrating thermo-optic bistability in an all-pass ring resonator device operating in a TM- mode. It has been shown in the literature [10,23] that when a laser of sufficient optical intensity is coupled on resonance into the cavity of a ring resonator, the absorbed portion of that optical intensity results in a change in temperature of the cavity which via the thermo-optic effect results in a shift of the resonant wavelength of the cavity. Modeling the change in refractive index resulting from a given optical power has been shown in [10–12,23]. The relation between the intensity of the optical wave in the cavity and the self-induced change in refractive index, Δn in time, t through induced temperature change and the film's thermo-optic coefficient is reproduced from Ref. [10] in Eqs. (1)–(3) below:

$$\frac{d\Delta n}{dt} = \Delta n_a - \frac{\Delta n}{t_c}. \tag{1}$$

Here Δn_a and t_c are defined as, the linear accumulation term and the characteristic time constant respectively.

$$\Delta n_a = \frac{\frac{dn}{dT}\, I\, \alpha}{2\rho C_p}, \tag{2}$$

where $\frac{dn}{dT}$, I, α, ρ, and C_p are the thermo-optic coefficient, Intensity, absorption coefficient, density, and specific heat respectively,

$$t_c = \frac{R^2 \rho C_p}{4k}, \tag{3}$$

where R and k are defined as the mode radius and thermal conductivity respectively. In the above $\rho \cong 2.2 g/cm^3$, $C_p \cong 0.76\ J/gK$, k ≅ 0.0014 W/cmK are taken from literature Refs. [10,12], while the mode radius R is taken to be the bend radius of the ring resonator cavity, $45\mu m$. The characteristic time constant t_c is both taken from measurements performed in section 5 and fit along with the unknowns $\frac{dn}{dT}$ and α, which is constrained by the overall propagation loss measured in section 3.

In this work we will explore this effect in high refractive index PECVD SRN, characterizing the thermo-optic coefficient by optical shift measurements as well as comparing it to a measurement of chip temperature. We will then perform time response measurements, estimate the relaxation time and deduce that it is indeed a thermal effect, as well as use this effect to demonstrate bi-stable optical switching.

Details of the PECVD SRN films deposition are described in our previous work [13]. Our device consists of a 311nm thick PECVD SRN device layer deposited onto 3um of wet thermal oxide on a silicon handling wafer. Our device design consisting of an input and output grating couplers along with a 45um bend radius all-pass ring resonator is patterned into the SRN device layer using electron-beam lithography of a 150nm thick HSQ soft mask. The developed HSQ mask is then used to transfer the device structure into the SRN device layer using reactive ion etching in an Oxford P100 etcher. After etching any remaining HSQ is removed using 1:10 buffered oxide etchant diluted in DI water. The devices are then clad with 1.5um of PECVD SiO_2. Figure 1 below shows an optical microscope image of our SRN all-pass ring resonator device consisting of a 45um bend radius ring with a width of 385nm coupled to a bus waveguide of width 385nm separated by a gap of 100nm.

Optics EXPRESS

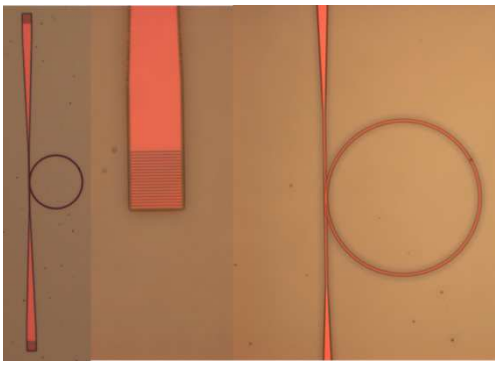

Fig. 1. Optical microscope image of the PECVD SRN 45um bend radius all-pass ring resonator device.

3. Low-power characterization

The transmission spectra from our SRN ring resonator device is first measured at low input optical powers in order to demonstrate that the spectra is symmetric at low input powers as well as determine the propagation loss and group index of our ring resonator device. To do so we couple an Agilent 81980B tunable laser to the input grating coupler and measure the output power using a Newport 918D-IG-OD3 detector connected to digital to analog converter and storage in the computer. We can then determine the transmission spectra by sweeping the wavelength of the Agilent tunable laser source and measuring the output power over time using the laser's output trigger to calibrate the wavelength at each moment along the measurement (more details on the measurement method can be found in our past work [13]).

Figure 2 shows the resulting normalized transmission spectra for the SRN ring resonator device operating in the TM-like mode. By fitting the transmitted optical spectra to a well-known line shape function, as in [24–25], using a root mean square fitting we can determine the propagation loss of the circulating mode, the group index, and the self-coupling coefficient of the bus waveguide. The results of the root mean square fitting of a single resonance can be seen as the blue dashed line in Fig. 2 corresponding to a group index of 3.522 ± 0.156, note that the FSR which is measured to be 2.38nm corresponds to a group index of 3.677 while a fitting of the single resonance on indicates as low as 3.3657, such uncertainty is considered in the margins of error presented on the fitted parameters as proper analysis of the resonances is harder in the nonlinear regime. A propagation loss of 3.38 dB/cm is found, with a self-coupling coefficient of 0.957 and a cross-coupling coefficient of 0.291. From this we estimate the field enhancement factor (FE) to be 5.1867 [10–12]. Additionally, it is important, to note that this loss value is the propagation loss of the mode circulating in the ring and thus includes all forms of loss such as bending, scattering, and absorption losses. Additional information on typical loss values in silicon-rich nitride films by the authors past works can be found in [13,14] with a more comprehensive view [17] as well as discussion on the usage of post-process annealing in LPCVD silicon-rich nitride films in [22]. As can be seen from these results under low input powers the line shape is symmetric indicating negligible contribution from self-induced thermo-optical bistability. Additionally, comparing these results to that of straight waveguides connected by grating couplers of the same design we estimate the insertion loss per grating coupler to be ~9.5dB.

Optics EXPRESS

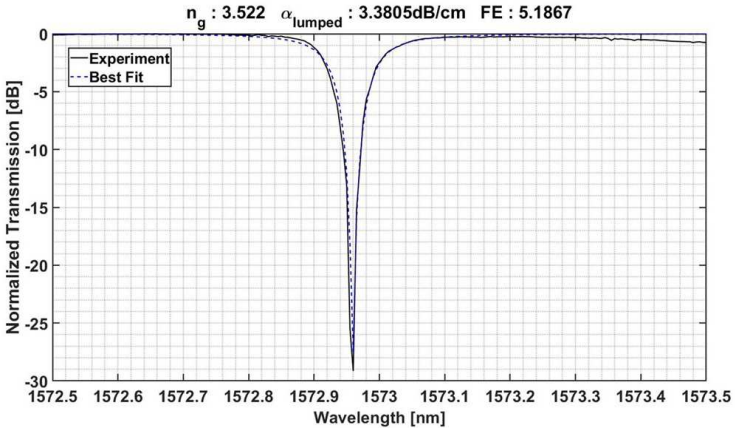

Fig. 2. Normalized transmission spectra at low input power for the SRN ring device operating in the TM-like mode. Shown is a fitting for the transmission spectra's line shape we determine the propagation loss to be 3.38 dB/cm for a group index of 3.522 ± 0.156.

4. Resonance shift

Work in literature [4,26] has shown that high optical intensities can result in bistability in a variety of in-waveguide configurations from Bragg gratings [27] to ring resonator devices [5]. Unlike in Si where competing effects contribute, the well-documented negligible nature of TPA [17,22] in silicon-rich nitride films at C-band allows measurements of optical shift to be attributed to temperature changes through the thermo-optic effect driven by linear absorption of a portion of the cavity intensity. The absorption coefficient induced by TPA is linearly dependent on the intensity while the resonant wavelength shift, as shown in Eq. (1) is dependent on the product of the absorption coefficient and the intensity in the steady state, resulting in a nonlinear relation between the TPA coefficient and resonant wavelength shift in its general form. As such the absorption which results in resonance shift seen here can be attributed to the linear absorption term which is a combination of various forms of absorption including material as well as interface state absorption, determining the exact contributions from each possible effect being beyond the scope of this work. Regardless, in a ring resonator device on-resonance light is coupled into the cavity where absorption induced heating increases the temperature of the ring causing a resonance shift due to the thermo-optic effect. In this section below we will compare measurements from optically induced resonant shifts to that of thermally heating the chip using a thermo-electric cooler (TEC). First, we demonstrate how this effect can induce a resonant wavelength shift in a ring resonator as a function of input optical power and creates an asymmetry in the line-shape of the resonator. Figure 3 below shows the transmission spectra of the 45um SRN ring resonator device as a function of input optical power.

Figure 3 shows a measurement of the transmission spectra, sweeping the laser's wavelength at a continuous sweep speed of 5nm/s. From these measurements the resonant wavelength of the ring resonator can be seen to have a linear dependence on the chip power. From these spectral measurements the shift rate is determined to be 91.98 pm/mW. Following methods laid in [10] by assuming that the absorbed optical intensity in the cavity creates an increase in temperature which shifts the resonant wavelength. Using this method we fit the shift in resonant wavelength vs chip power for the thermo-optic coefficient, absorption coefficient, and the thermal relaxation time. Constraining the absorption coefficient to be less than the measured propagation loss measured in Section 3, as this measured value is a combination of all forms of loss in the ring cavity, we determine the thermo-optic coefficient to be $(2.12 \pm 0.125) \times 10^{-4}$ /°C. It is important

Optics EXPRESS

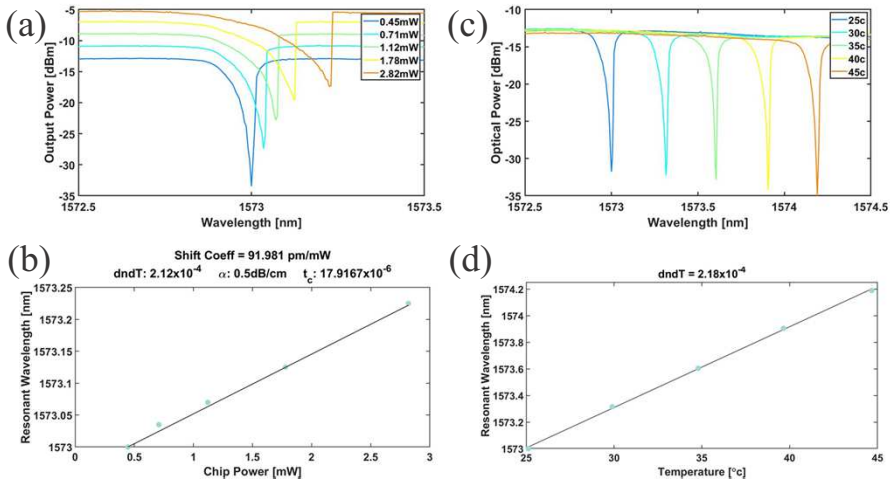

Fig. 3. (a) Transmission spectra of a 45um SRN ring resonator for the corresponding on-chip powers in (b). Notice how at the lowest laser power presented the asymmetry is reduced and as the laser power increases the resonant wavelength red-shifts and the resonance becomes increasingly asymmetric. (b) Measured resonant wavelength vs chip power in mW along with a fit line showing a shift coefficient of 91.98 pm/mW for a loss coefficient of 0.5dB/cm. (c) Transmission spectra of a 45um SRN ring resonator as a function of stage temperature from 25°C to 45°C. (d) Measured resonant wavelength versus temperature.

to note that due to inherent uncertainties in the absorption coefficient the uncertainty as estimated from the optical shift is larger than that estimated by stage temperature. Second, we measure the transmission spectra as a function of stage temperature, comparing it to the measurement versus chip power. Figure 3(c) shows the measured transmission spectra for stage temperatures from 25°C to 45°C. From these measurements the resonant wavelength of the ring resonator can be seen to have a linear dependence on stage temperature from which we can estimate the thermo-optic coefficient to be $(2.18 \pm 0.09)\times10^{-4}$/°C. Comparing these two measurements of the thermo-optic coefficient we find good agreement in the estimated coefficient. Additionally, it is important to note that it is more challenging to fit for the parameters of interest in the nonlinear regime due to deformation in the resonance and it would be useful for a future work to explore this space further for example as a function of sweep speed of the laser in addition to chip-power.

5. Time response

In this section we will measure the temporal response of the self-induce thermo-optic effect in order to demonstrate that it is indeed thermal in nature, as well as estimate the specific thermal relaxation time of our SRN ring resonator device. As we demonstrated in the previous section, the resonant wavelength of the ring resonator shifts as a function of optical power. In order to measure the temporal response of our device we modulate the intensity of the input optical wave using a pulsed sawtooth wave of increasing frequency in the range of 1kHz to 150kHz, with a delay of 10ms between pulses to allow time for the cavity to relax back to equilibrium. When the wavelength of the laser is fixed at the maxima between resonance positions, the transmitted optical power simply tracks the sawtooth wave of the input, which we refer to as a baseline. Next we set the resonant wavelength detuned by +40pm from the resonant wavelength of the device (1576.6nm). Since increasing optical power during the ramp of the sawtooth causes the filter resonance to red shift past the set laser wavelength, the optical transmission power will show a sudden drop followed by its increase again until the end of the ramp when the output

Optics EXPRESS

optical power will drop reaching the baseline. After the sawtooth ramp ends and it returns to the initial optical power the resonator returns to equilibrium (i.e., baseline) over a period of thermal relaxation.

Figure 4 shows a measurement of the transmitted optical power normalized to the transmission at t = 0, for the baseline and near resonance case for frequencies from 1kHz to 150kHz measured using a Hewlett Packard 11982A lightwave converter and a Tektronic TDS3014C digital oscilloscope. As can be observed from Fig. 4, at lower frequencies, such as in the 1kHz measurement, there is a sharp drop in the transmitted power around t = 500us as expected and then at t = 1000us when the sawtooth returns to its initial state there is another sharp drop as the cavity returns to equilibrium. As the frequency of the ramp is increased it becomes clear that after the sawtooth returns to its initial state the cavity requires a relaxation time of ~18.7us to return to equilibrium. If we compare this to the photon lifetime of a 20,000-quality factor ring resonator [25,28], $\tau_{ph} = \frac{2Q}{\omega_0}$, which is ~33ps we find this clearly indicates our measured relaxation time corresponds to thermal relaxation confirming this as a thermo-optic shift.

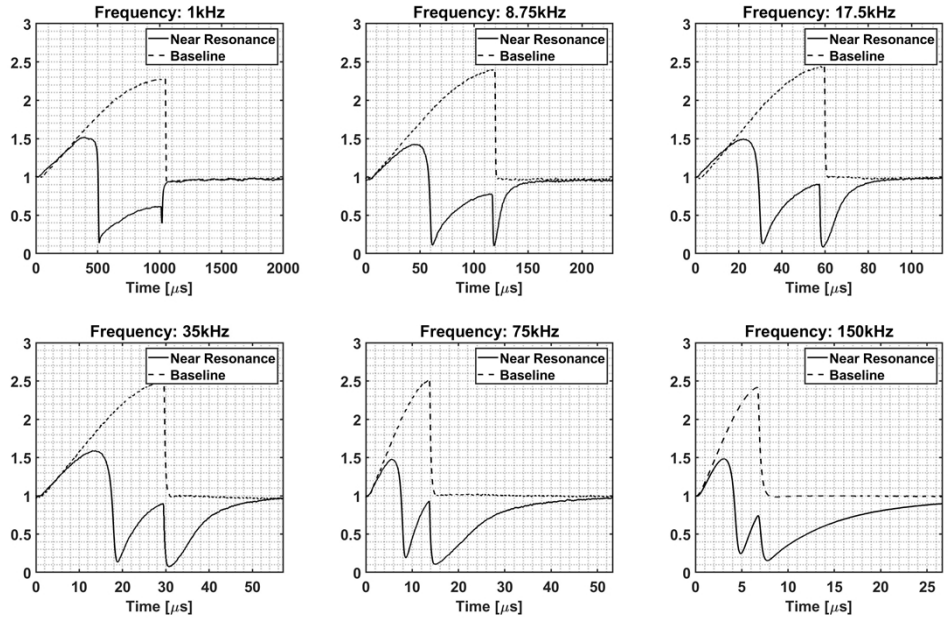

Fig. 4. Transmission as a function of time for the 'baseline' curve as well as the 'near resonance' case for ramp 'frequencies' from 1kHz up to 150kHz.

6. Bi-stable optical switching

In the previous sections we have demonstrated optically induced thermo-optic shifts in a PECVD SRN ring resonator determining the thermo-optic coefficient to be (2.12 ± 0.125) x 10^{-4}/°C and the confirmed this to be due to a thermo-optic effect by time response measurements. Finally, in this section we utilize the SRN ring resonator device to demonstrate that the transmitted optical power as a function of input power exhibits a bi-stable regime which is used to demonstrate bi-stable optical switching.

The left-hand plot in Fig. 5 shows an example of the transmission spectra of the ring resonator device at two different on-chip optical powers, 0.45mW (P_{laser} = 6dBm) in black and 1.12mW (P_{laser} = 10dBm) in teal. As shown in previous sections, as the input power is increased the resonance becomes more asymmetric and the resonance red shifts. The right-hand plot in

Optics EXPRESS

Fig. 5 is taken by positioning the laser red-shifted from the resonant wavelength at 0.45mW (P_{laser} = 6dBm) by +40pm, the transmitted optical power is then measured as a function of input power. The input power is first swept upwards from the minimum power 0.45mW (P_{laser} = 6dBm) to the maximum power of 2.8mW (P_{laser} = 14dBm), then the input power is swept downwards from 2.8mW (P_{laser} = 14dBm) to 1.12mW (P_{laser} = 10dBm), after which the input power is linearly looped from 1.12mW (P_{laser} = 10dBm) to 1.78mW (P_{laser} = 12dBm) to 1.12mW (P_{laser} = 10dBm) three times before finally being swept downwards from 1.12mW (P_{laser} = 10dBm) to 0.45mW (P_{laser} = 6dBm) again. As can be seen by the black connecting lines between the teal datapoints, outside of the 1.12mW to 1.78mW region of on-chip input power the on-chip output power is stable. Inside this region the power can jump between two bi-stable states. Additionally, if the input power is swept upwards from the below this bi-stable region upwards into it, the output power can be placed in a stable state in the upper branch. If the input power is swept from this state upwards above the maximum of the bi-stable region and then back downwards it can be switched into a stable state in the lower branch. Finally, if the input power is swept downwards from this position below the bi-stable region and then back upwards it can be again placed into a stable state in the upper branch. Using this methodology, we demonstrate bi-stable optical switching, showing a 0,1,0,1,0,1 bit sequence, using a control sequence at the input power. The switching is performed by either 'pulsing' the input power or lower, and then returning the input power to the bias state with a finite ΔP_{in} differential of 0.4dB.

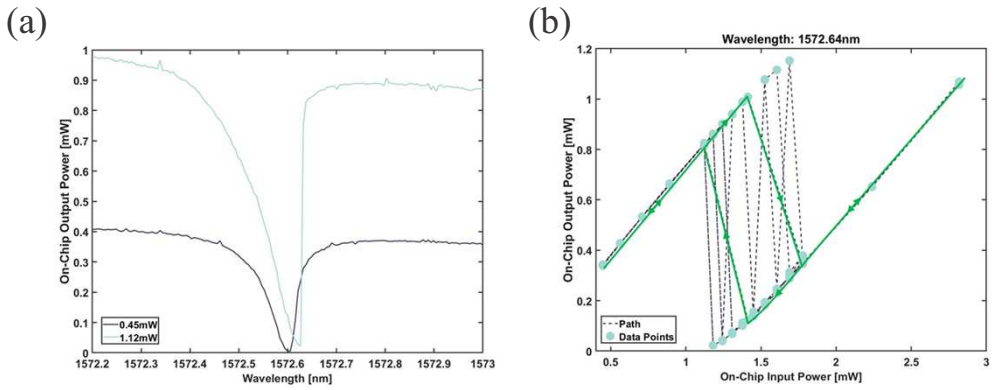

Fig. 5. (a) The transmission spectra of the ring resonator device at two different on chip powers, in black 0.45mW (P_{laser} = 6dBm), and in teal 1.12mW (P_{laser} = 10dBm). Notice how as the input power is increased the resonance becomes more asymmetric and the resonance point red shifts. (b) Transmitted optical power as a function of input optical power demonstrating how there is a region of input power, from approximately 10mW, to 16mW, where multiple solutions are possible. Depending on the way the input power is scanned the transmission can be in either of the branches and be either stable (green loop) or unstable (dashed light-blue lines).

The result of these measurements can be seen in Fig. 6 as normalized transmission over time for the 0,1,0,1,0,1 bit sequence, where each 'bit' is held for 120s, and each sample point is averaged for 10ms. As the result shows it is possible to stable switch between the two branches shown in Fig. 5 using a control sequence and once switched the output is stable in the new state with 10dB of extinction achieved between the two states. Although as we have demonstrated this is a result of the thermo-optic effect, and so speed is limited, it is still a useful demonstration of the ability to cleanly switch between the two bi-stable states and the required input optical power in a high refractive index PECVD SRN all-pass ring resonator and through novel architectures

Optics EXPRESS

and control schemes such as that in [29,30] the interplay between this thermally induced effect and the Kerr effect can be explored to develop an ultra-fast bi-stable device.

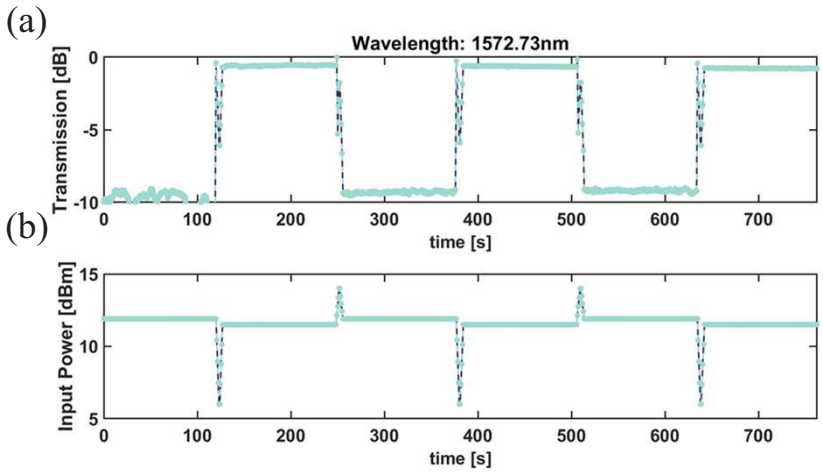

Fig. 6. (a) Normalized transmission as a function of time for a '0,1,0,1,0,1' bit sequence. The two stable output states can be switched between using a control sequence on the input power that begins and ends at the same power level with a finite ΔP_{in} differential of 0.4dB. (b) Input power showing the control sequence as well as the ΔP_{in} differential of 0.4dB.

7. Conclusion

Optically bi-stable devices are of keen interest for development of optical logic components as well as potentially for other devices such as photonic thermometers [12]. In the past, optical bistability was shown in silicon devices. However, with growing interest in use of silicon nitride devices due to their low loss and negligible TPA, it becomes interesting to explore their ability to realize optical bistability. In recent years it has also been shown that by enhancing the silicon content in silicon nitride films, the second and third order nonlinear susceptibilities as well as the thermo-optic coefficient are increased while maintaining a variety of benefits from stoichiometric silicon nitride, such as the negligible TPA. Despite this however, research into optical bistability and devices design to exploit it have not significantly adopted high silicon content SRN films despite their advantages.

In this manuscript we have presented a study of self-induced thermo-optic bistability in PECVD SRN. We have shown that such PECVD SRN films achieve low propagation loss of 3.07dB/cm and determined the thermo-optic coefficient to be $(2.12 \pm 0.125)\times10^{-4}$/°C by a comparison of optically induced resonance shift and thermal heating. time response measurements were performed which demonstrate a relaxation time of 18.7us at up to 150kHz. Finally, we demonstrated bi-stable optical switching showing that there exists a bi-stable region between 10dBm and 12dBm in which two possible output power states are possible which can be either stable or unstable. PECVD SRN has the potential to enhance optically bi-stable devices by enabling more sensitive temperature sensors due to its enhanced TOC, as well as potentially open new avenues for Kerr based optical bistability if used in an add-drop configuration [11]. In this manuscript we have explored the thermo-optic portion of bistability in PECVD SRN demonstrating it to have significant advantages over stoichiometric nitride based approaches. PECVD SRN is a promising material platform which deserves further research into utilizing it for Kerr based potentially ultrafast bistability and how that interacts with its slower thermo-optic bistability [31].

Optics EXPRESS

Funding. Cymer; Advanced Research Projects Agency - Energy; U.S. Department of Energy (DE-SC0019273); San Diego Nanotechnology Institute (NSF grant ECCS-1542148, NSF grant ECCS-2025752); Army Research Office; National Science Foundation (CBET-1704085, DMR-1707641, NSF ECCS-180789, NSF ECCS-190184, NSF ECCS-2023730); Office of Naval Research; Defense Advanced Research Projects Agency (DSO NLM, NAC).

Acknowledgments. We thank all of UCSD's nano3 cleanroom staff and Dr Maribel Montero for their assistance with sample fabrication.

Disclosures. The authors declare no conflicts of interest.

Data availability. Data underlying the results presented in this paper are not publicly available at this time but may be obtained from the authors upon reasonable request.

References

1. P. Sethi and S. Roy, "Ultrafast all-optical flip-flops, simultaneous comparator-decoder and reconfigurable logic unit with silicon microring resonator switches," IEEE J. Sel. Top. Quantum Electron. **20**(4), 118–125 (2014).
2. P. Keshtkar, M. Miri, and N. Yasrebi, "Low power, high speed, all-optical logic gates based on optical bistability in graphene-containing compact microdisk resonators," Appl. Opt. **60**(24), 7234–7242 (2021).
3. P. Nadimi, D. D. Caviglia, and E. Di Zitti, "Exploiting silicon-on-insulator microring resonator bistability behavior for all optical set-reset flip-flop," Int. J. Phys. Math. Sci. **6**(11), 1485–1489 (2012).
4. V. R. Almeida and M. Lipson, "Optical bistability on a silicon chip," Opt. Lett. **29**(20), 2387–2389 (2004).
5. A. A. Nikitin, I. A. Ryabcev, A. A. Nikitin, A. V. Kondrashov, A. A. Semenov, D. A. Konkin, A. A. Kokolov, F. I. Sheyerman, L. I. Babak, and A. B. Ustinov, "Optical bistable SOI micro-ring resonators for memory applications," Opt. Commun. **511**, 127929 (2022).
6. G. Priem, P. Dumon, W. Bogaerts, D. Van Thourhout, G. Morthier, and R. Baets, "Optical bistability and pulsating behaviour in Silicon-On-Insulator ring resonator structures," Opt. Express **13**(23), 9623–9628 (2005).
7. I. D. Rukhlenko, M. Premaratne, and G. P. Agrawal, "Analytical study of optical bistability in silicon ring resonators," Opt. Lett. **35**(1), 55–57 (2010).
8. P. Sun and R. M. Reano, "Low-power optical bistability in a free-standing silicon ring resonator," Opt. Lett. **35**(8), 1124–1126 (2010).
9. S. Chiangga, S. Pitakwongsaporn, T. D. Frank, and P. P. Yupapin, "Optical bistability investigation in a nonlinear silicon microring circuit," J. Lightwave Technol. **31**(7), 1101–1105 (2013).
10. K. Ikeda, R. E. Saperstein, N. Alic, and Y. Fainman, "Thermal and Kerr nonlinear properties of plasma-deposited silicon nitride/silicon dioxide waveguides," Opt. Express **16**(17), 12987–12994 (2008).
11. Wataru Yoshiki and Takasumi Tanabe, "Add-drop system for Kerr bistable memory in silicon nitride microrings," arXiv preprint arXiv:1308.6042 (2013).
12. C. Zhang, G.-G. Kang, J. Wang, S. Wan, C.-H. Dong, Y.-J. Pan, and J.-F. Qu, "Photonic thermometer by silicon nitride microring resonator with milli-kelvin self-heating effect," Measurement **188**, 110494 (2022).
13. A. Friedman, H. Nejadriahi, R. Sharma, and Y. Fainman, "Demonstration of the DC-Kerr effect in silicon-rich nitride," Opt. Lett. **46**(17), 4236–4239 (2021).
14. H. Nejadriahi, A. Friedman, R. Sharma, S. Pappert, Y. Fainman, and P. Yu, "Thermo-optic properties of silicon-rich silicon nitride for on-chip applications," Opt. Express **28**(17), 24951–24960 (2020).
15. H.-H. Lin, R. Sharma, A. Friedman, B. M. Cromey, F. Vallini, M. W. Puckett, K. Kieu, and Y. Fainman, "On the observation of dispersion in tunable second-order nonlinearities of silicon-rich nitride thin films," APL Photonics **4**(3), 036101 (2019).
16. M. W. Puckett, R. Sharma, H.-H. Lin, M.-h. Yang, F. Vallini, and Y. Fainman, "Observation of second-harmonic generation in silicon nitride waveguides through bulk nonlinearities," Opt. Express **24**(15), 16923–16933 (2016).
17. D. T. H. Tan, K. J. A. Ooi, and D. K. T. Ng, "Nonlinear optics on silicon-rich nitride: a high nonlinear figure of merit CMOS platform," Photonics Res. **6**(5), B50–B66 (2018).
18. B.-U. Sohn, J. W. Choi, D. K. Ng, and D. T. Tan, "Optical nonlinearities in ultra-silicon-rich nitride characterized using z-scan measurements," Sci. Rep. **9**(1), 1–7 (2019).
19. K. J. A. Ooi, D. K. T. Ng, T. Wang, A. K. L. Chee, S. K. Ng, Q. Wang, L. K. Ang, A. M. Agarwal, L. C. Kimerling, and D. T. H. Tan, "Pushing the limits of CMOS optical parametric amplifiers with USRN: Si7N3 above the two-photon absorption edge," Nat. Commun. **8**(1), 1–10 (2017).
20. C. J. Krückel, A. Fülöp, Z. Ye, and P. A. Andrekson, "Optical bandgap engineering in nonlinear silicon nitride waveguides," Opt. Express **25**(13), 15370–15380 (2017).
21. D. K. Ng, H. Gao, P. Xing, G. F. Chen, X. X. Chia, Y. Cao, K. Y. Ong, and D. T. Tan, "Enhanced photonics devices based on low temperature plasma-deposited dichlorosilane-based ultra-silicon-rich nitride (Si8N)," Sci. Rep. **12**(1), 1–13 (2022).
22. C. Lacava, S. Stankovic, A. Z. Khokhar, T. Dominguez Bucio, F. Y. Gardes, G. T. Reed, D. J. Richardson, and P. Petropoulos, "Si-rich silicon nitride for nonlinear signal processing applications," Sci. Rep. **7**(1), 22 (2017).
23. A. A. Nikitin, A. V. Kondrashov, V. V. Vitko, I. A. Ryabcev, G. A. Zaretskaya, N. A. Cheplagin, D. A. Konkin, A. A. Kokolov, L. I. Babak, A. B. Ustinov, and B. A. Kalinikos, "Carrier-induced optical bistability in the silicon micro-ring resonators under continuous wave pumping," Opt. Commun. **480**, 126456 (2021).

Optics EXPRESS

24. R. Sharma, M. W. Puckett, H.-H. Lin, A. Isichenko, F. Vallini, and Y. Fainman, "Effect of dielectric claddings on the electro-optic behavior of silicon waveguides," Opt. Lett. **41**(6), 1185–1188 (2016).
25. W. Bogaerts, P. De Heyn, T. Van Vaerenbergh, K. De Vos, S. K. Selvaraja, T. Claes, P. Dumon, P. Bienstman, D. Van Thourhout, and R. Baets, "Silicon microring resonators," Laser Photonics Rev. **6**(1), 47–73 (2012).
26. P. Xing, D. Ma, L. C. Kimerling, A. M. Agarwal, and D. T. Tan, "High efficiency four wave mixing and optical bistability in amorphous silicon carbide ring resonators," APL Photonics **5**(7), 076110 (2020).
27. A. Grieco, B. Slutsky, D. T. Tan, S. Zamek, M. P. Nezhad, and Y. Fainman, "Optical bistability in a silicon waveguide distributed Bragg reflector Fabry–Perot resonator," J. Lightwave Technol. **30**(14), 2352–2355 (2012).
28. Z. Zhang, M. Dainese, M, Chacinski, L. Wosinski, and M, Qiu, "High-quality-factor micro-ring resonator in amorphous-silicon on insulator structure," (2008): 329–332.
29. B. A. Daniel and G. P. Agrawal, "Phase-switched all-optical flip-flops using two-input bistable resonators," IEEE Photonics Technol. Lett. **24**(6), 479–481 (2012).
30. M. F. Yanik, S. Fan, and M. Soljačić, "High-contrast all-optical bistable switching in photonic crystal microcavities," Appl. Phys. Lett. **83**(14), 2739–2741 (2003).
31. W. Yoshiki and T. Tanabe, "Analysis of bistable memory in silica toroid microcavity," J. Opt. Soc. Am. B **29**(12), 3335–3343 (2012).